

Fast temporal phase unwrapping method for the fringe reflection technique based on the orthogonal grid fringes

Bo Li,^{1,2,*} SUODONG MA,^{3,4} AND YANG ZHAI^{1,2}

¹Nanjing Institute of Astronomical Optics & Technology, National Astronomical Observatories, Chinese Academy of Sciences, Nanjing 210042, China

²Key Laboratory of Astronomical Optics & Technology, Nanjing Institute of Astronomical Optics & Technology, Chinese Academy of Sciences, Nanjing 210042, China

³College of Physics, Optoelectronics and Energy, Soochow University, Suzhou 215006, China

⁴Key Lab of Advanced Optical Manufacturing Technologies of Jiangsu Province & Key Lab of Modern Optical Technologies of Education Ministry of China, Soochow University, Suzhou 215006, China

*Corresponding author: bli@niaot.ac.cn

Received 5 May 2015; revised 18 June 2015; accepted 18 June 2015; posted 19 June 2015 (Doc. ID 240353); published 8 July 2015

In traditional temporal phase unwrapping (TPU) algorithms, wrapped phases with different spatial frequencies are obtained from several groups of phase shift fringes to calculate the unwrapped phase. Therefore, the necessary quantity of captured fringes is very large, especially for the fringe reflection technique (FRT), since a pair of phases should be unwrapped to get the slopes of two perpendicular directions. In this paper, we propose a fast TPU algorithm based on the orthogonal grid fringes by which only one image is needed to extract the two integer phases for each frequency instead of two groups of phase shift fringes, and then they can be added into the wrapped phases separately to complete the unwrapping. There are ridge errors in the direct unwrapped phases, but they are significantly suppressed by our pseudo-phase-shift strategy without any extra captured fringes. The proposed method is robust and effective where the fringe amount used for unwrapping is only 1/4 of the previous similar algorithm and 1/6–1/8 of the traditional TPU methods. The detailed comparison of measurement time is also given, which demonstrate that the FRT measurement can be accelerated in most cases by our method. The algorithm is validated by the experiments, which still works well for the severely defocusing fringes or complex specimen. © 2015 Optical Society of America

OCIS codes: (120.0120) Instrumentation, measurement, and metrology; (100.2650) Fringe analysis; (120.6650) Surface measurements, figure.

<http://dx.doi.org/10.1364/AO.54.006282>

1. INTRODUCTION

Fringe reflection technique (FRT) [1–6], which is also called phase measuring deflection (PMD) or software configurable optical test system (SCOTS), has become a popular method for measuring the specular surface shape. In a typical FRT system, the standard fringes shown in an LCD screen are reflected by the specular samples, and then the distorted fringes are captured by a camera. The two perpendicular slopes of the sample can be extracted from the phases of the captured fringes, and then the surface can be reconstructed.

Phase unwrapping is an important process of various phase retrieving techniques including the FRT, which can be divided into temporal [7–10] and the spatial methods [11]. The spatial ones use only one wrapped phase, but they suffer from sensitivity to noises, calculation complexity, and the difficulty in unwrapping the discontinue area, since the unwrapped phase

value of one pixel is emulated from the neighborhood locally [12,13] or globally [14,15]. The unwrapping starting point may also need to be carefully selected by using specialized strategies [16]. By contrast, temporal phase unwrapping (TPU) methods use several wrapped phase values for a given pixel location to calculate the unwrapped phase value. These wrapped phase values are obtained from the corresponding locations in the successively captured images of differing fringe spatial frequencies. Due to the isolated unwrapping calculation of each pixel (i.e., the unwrapped phase of one pixel is decided by the wrapped phase values in the same location with different spatial frequencies, independently of neighboring pixels' phase values), the temporal methods have the advantages of calculation simplicity and robustness and the ability to unwrap the data in the separated zones [9]. Thus, it is often the better choice in the fields of fringe projection technique (FPT) and FRT [17]. On

the other hand, its main disadvantage is the significant increment of the capture time, since several groups of phase shift fringes are captured to obtain the necessary wrapped phase with different spatial frequencies [10,18]. In addition, in the cases of high-speed measurement, more processing time also should be considered, and extra hardware may therefore be needed. Compared with the FPT, this problem is more critical in the FRP because a pair of phases should be calculated to obtain the perpendicular slopes of the x and y directions, which means the amount of captured fringes is even twice as FPT.

The basic flow chart of TPU, which is a recursion process, can be seen in Fig. 1 [10]. The integer phase (i.e., $2\pi L$, where L is the integer) is first obtained from the wrapped phase with current spatial frequencies and the unwrapped phase with lower frequencies, and then the integer phase is added on the wrapped phase to obtain the unwrapped phase. For the lowest spatial frequency, the wrapped phase should equal to the unwrapped phase whose peak-to-valley value is less than 2π , and the recursion calculation can be realized. Considering the integer phase is extracted from the first $n - 1$ groups of phase shift fringes and the detailed wrapped phase (from $-\pi$ to π) is extracted from the last one in the traditional TPU algorithms, the former can be reduced to only one binary for each frequency while not a period of phase shift fringes (three to four images typically), which is also sufficient to theoretically calculate the integer phase. The combination of binary fringes and phase shift ones was previously used by Sansoni *et al.* [19] in the field of FPT, and afterward a modified method suitable for the FRT was proposed by Butel *et al.* [20]. However, the simplification effect of [20] is still limited by the separated unwrapping of the two perpendicular phases and the extra captured fringes to correct the ridge errors, which just reduces the fringes amount from six to eight frames to four for each frequency.

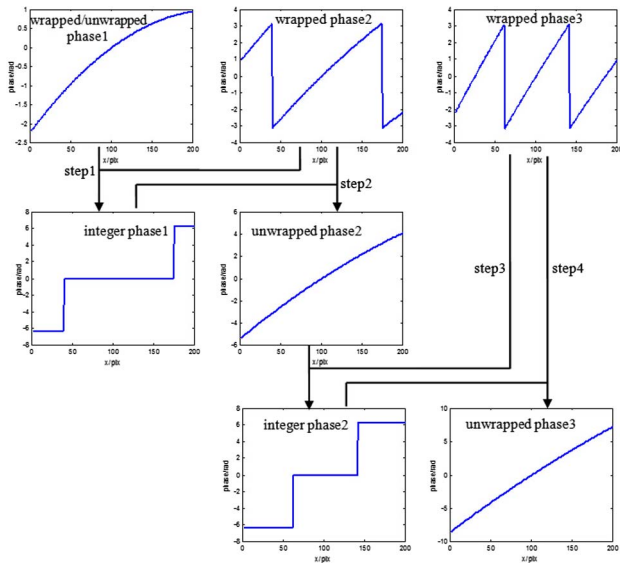


Fig. 1. Flow chart of the temporal phase unwrapping. Step 1 and 3: The integer phase is obtained from the wrapped phase with current spatial frequency and the unwrapped phase with lower frequency. Step 2 and 4: The integer phase is added on the wrapped phase to obtain the unwrapped phase.

Therefore, a method based on the orthogonal grid fringes (OGF) is proposed in this paper to greatly reduce the capture time in TPU. There are three significant differences between our method and the binary fringe method, so that only 1/4 number of the captured fringes are used for unwrapping: (1) The standard phases along the x and y directions in each fringes frequency are encoded into one OGF image with four gray levels, rather than being processed separately by two binary fringes. Then, the two integer phases can be extracted from one captured fringe image, so the capture time can be further reduced by half. The technique of orthogonal fringes was once used in FRT by some authors [21,22] to obtain the slopes of x and y directions by one measurement, but in these works sinusoid fringes were combined rather than binary fringes, and these fringes were not used for phase unwrapping. (2) Our OGF method expands on binary fringes by introducing intermediate gray levels and corrects the nonuniform intensity of the captured fringe images to avoid gray-level identification ambiguities. (3) In practice, the ridge errors caused by the gray ambiguity in the captured binary or OGF fringes are evident, which means a refining process is necessary. Reference [20] uses the phase shift binary fringes to solve this problem, which double the captured images amount, while our method uses a pseudo-phase-shift strategy without a need for capturing any extra supplementary images.

2. PRINCIPLE AND ALGORITHM

A. Basic Principle

First, we define φ_W and φ_U as the symbols of the wrapped phase and the unwrapped phase of a pixel, respectively, so

$$\varphi_U = \varphi_W + 2\pi L, \tag{1}$$

where L is the integral coefficient of 2π to be calculated by the phase unwrapping. The term of $2\pi L$ is called the integer phase in this paper.

In TPU methods, φ_U can be determined by a general recursive formula [10]:

$$\varphi_U(t_2) = \varphi_W(t_2) - 2\pi \cdot \text{NINT} \left[\frac{\varphi_W(t_2) - \varphi_U(t_1) \cdot T(t_1)/T(t_2)}{2\pi} \right], \tag{2}$$

where t_1 and t_2 represent the sequences' number of different groups, T is the fringes' periods (i.e., the reciprocal of the frequency). NINT is the operator to obtain the nearest integer, which is defined by

$$\text{NINT}[\pm(A + a)] = \begin{cases} \pm A, & 0 < a < 0.5 \\ \pm(A + 1), & 0.5 \leq a < 1 \end{cases} \tag{3}$$

where A is the positive integer and a is the positive decimal. In Eq. (2), there is no limitation for the temporal sequence, which means the frequencies (fringe number) of the t -th group can be set obeying the exponential, reversed exponential, or linear sequence in traditional TPU [10], but only the exponential or reversed exponential sequence is available for the binary fringes methods.

The binary fringes vary along the x direction and can be given by

$$I_x(x, y, t) = \begin{cases} 0, & \text{FLOOR}[x/T_x(t)] = \text{odd} \\ 1, & \text{FLOOR}[x/T_x(t)] = \text{even} \end{cases} \quad (4)$$

where the operator FLOOR denotes rounding to the integer smaller than the parameter. And the fringe frequency $1/T_x$ is set to obey the exponential sequence:

$$T_x(t) = T_x(1)/2^{t-1}. \quad (5)$$

There is almost no difference for the method of this paper if the reversed exponential sequence is used, so it will not be discussed to avoid the redundancy.

Similarly, the binary fringes vary along the y direction:

$$I_y(x, y, t) = \begin{cases} 0, & \text{FLOOR}[y/T_y(t)] = \text{odd} \\ 1, & \text{FLOOR}[y/T_y(t)] = \text{even} \end{cases} \quad (6)$$

It is notable that the gray levels of all images in this paper are normalized to $[0,1]$. In the last group of fringes, the phase shift fringes are shown in the screen to obtain the main value of the phase using the standard phase shift algorithm (PSA) [23], and their periods should be a half of T_x and T_y , respectively.

Then, the OGF is generated by combining I_x and I_y :

$$G(t) = \begin{cases} 0, & I_x(t) = 0 \text{ and } I_y(t) = 0 \\ v_1, & I_x(t) = 1 \text{ and } I_y(t) = 0 \\ v_2, & I_x(t) = 0 \text{ and } I_y(t) = 1 \\ 1, & I_x(t) = 1 \text{ and } I_y(t) = 1 \end{cases} \quad (7)$$

where v_1 and v_2 are the gray levels to mark the relative areas in the OGF image ($0 < v_1 < v_2 < 1$), and the dependencies on x and y are omitted for brevity. In the ideal case, v_1 and v_2 are $1/3$ and $2/3$, respectively, to clearly distinguish the four gray levels. However, their values should be adjusted to

$$\begin{cases} v'_1 = v_1^\gamma \\ v'_2 = v_2^\gamma \end{cases} \quad (8)$$

due to the gamma distortion of the display and the camera in the FRT system in which γ is the gamma coefficient [17,24].

To obtain the integer phases, the captured OGF image $G'(t)$ at first should be decomposed to two binary fringes. This reversed operation of Eq. (7) can be written as

$$\begin{aligned} I_x(t) &= \begin{cases} 0, & G(t) \leq \text{thr2} \\ 1, & G(t) = \text{thr2} \end{cases} \\ I_y(t) &= \begin{cases} 0, & \text{thr1} < G(t) \leq \text{thr2} \text{ or } G(t) > \text{thr3} \\ 1, & \text{thr2} < G(t) \leq \text{thr3} \text{ or } G(t) > \text{thr1} \end{cases} \end{aligned} \quad (9)$$

where the three thresholds thr1 , thr2 , and thr3 can be set manually or calculated automatically based on the histogram of the captured OGF. The examples of combining two binary fringes into an OGF and its reversed operation, which decompose a captured OGF to two binary fringes, are shown in Fig. 2.

Then, the integer wrapped phase can be directly determined by the retrieved binary fringes:

$$\varphi_W(t) = I(t), \quad t = 1, 2, \dots, t_{\max} - 1, \quad (10)$$

where the subscripts x and y of φ_W and I are both omitted, since the equations are all the same in these two cases. It is evident that there is only the integer information in the wrapped phase $\varphi_W(t)$ if $t < t_{\max}$, which is different from the traditional TPU algorithms. And the final unwrapped phase can be obtained by the formula:

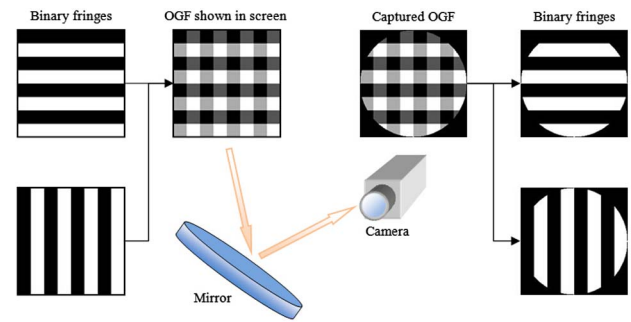


Fig. 2. Combining two binary fringes into an OGF and the reversed operation.

$$\varphi_U = \varphi_W(t_{\max}) + 2\pi \cdot \sum_{t=1}^{t_{\max}-1} 2^{t_{\max}-t-1} \cdot \text{NINT}[\varphi_W(t)] \quad (11)$$

or the recursive formula, as in Eq. (2), since the exponential sequence is a specific form of TPU. As previously defined, the wrapped phases of the last group $\varphi_W(t_{\max})$ are obtained from the phase shift fringes by the standard PSA [23].

Although the basic algorithm of the OGF is simple and clear, as previously explained, it does not work well in actual conditions if no enhancement strategy is applied. In the following two subsections, we will use the nonuniform intensity correction and the pseudo-phase-shift method to improve the algorithm significantly without any extra captured fringes quantity.

B. Nonuniform Intensity Correction

The nonuniform intensity of the captured fringes is the first factor to affect the result, which will reverse the magnitude relation of the four gray levels in the OGF, so the identification process of Eq. (9) using the global threshold will be wrong. For example, in two rows of an actual captured OGF image, as shown in Fig. 3, the first gray level around the image edge is smaller than the second one near the center instead of the ideal magnitude relation ($1^{\text{st}} > 2^{\text{nd}} > 3^{\text{rd}} > 4^{\text{th}}$), so they cannot be distinguished reliably by using the gray threshold. To avoid this error, the background or modulation of the fringes can be calculated as the correction reference [25] using the

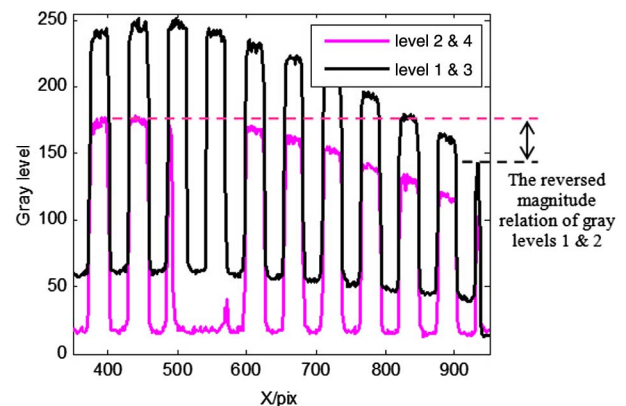


Fig. 3. Wrong identification of the gray level caused by the intensity nonuniform.

least-squares method from the phase shift fringes. The modulation is selected here for its ability to reject the invalid points, which can be calculated by

$$M(x, y) = \sqrt{\left(\sum_{n=1}^N s_n \cos \frac{2\pi n}{N}\right)^2 + \left(\sum_{n=1}^N s_n \sin \frac{2\pi n}{N}\right)^2}, \quad (12)$$

where s_n is the n -th phase shift fringes. Here, the N steps of phase shift values are assumed uniform in a 2π period, which is very common in PSA [23]. Unfortunately, this distribution is easy to be affected by the gamma distortion and image noises [26], so it cannot be used to correct the nonuniform intensity of the OGF directly. Alternatively, it will be much more reliable if this distribution is fitted to a given model. In the cases of regular pupil, the nonuniform distribution usually can be approximately represented by a Gauss function:

$$\text{Gauss}(x, y) = \exp\left\{-\left[\frac{(x-x_0)^2}{\varepsilon^2} + \frac{(y-y_0)^2}{\eta^2}\right]\right\}, \quad (13)$$

where the four parameters x_0 , y_0 , ε , and η are needed to be determined by solving the least-squares equations:

$$\begin{bmatrix} x^2 & -2x & y^2 & -2y & 1 \end{bmatrix} \begin{bmatrix} 1/\varepsilon^2 \\ x_0/\varepsilon^2 \\ 1/\eta^2 \\ y_0/\eta^2 \\ x_0^2/\varepsilon^2 + y_0^2/\eta^2 \end{bmatrix} = -\ln M(x, y). \quad (14)$$

The four unknown parameters of the Gauss function can be easily solved from this linear least-squares equation, and then the nonuniform intensity can be corrected well by dividing Gauss(x, y):

$$I'_x(x, y, t) = \frac{I_x(x, y, t)}{\text{Gauss}(x, y)}, \quad I'_y(x, y, t) = \frac{I_y(x, y, t)}{\text{Gauss}(x, y)}. \quad (15)$$

Finally, the corrected OGF images I'_x and I'_y can be used to replace I_x and I_y in Eq. (9) to evade the wrong identification.

It is notable that the assumption of Gauss intensity distribution is only suitable for the simple objects, which contain the most optical mirrors with regular pupils and a relative small dynamic range. For the complex specimen, however, the intensity distribution can be irregular. Therefore, three calibration images with the uniform gray levels equaling to the three gray thresholds in Eq. (9), respectively, should be projected first, and then the captured images can be used to determine the correct threshold in each pixel. This kind of sample will be presented in our third experiment, as described in the Experiments section.

C. Processing the Ambiguous Gray Levels

The ambiguity of gray levels is the second error source to be corrected. It is evident that the grid edges are not clear in the captured OGF images because the captured fringes are always defocused in the FRT system, which is also effected by other imaging imperfections of the camera. The blur generates many ridge errors in the direct unwrapped results around the corresponding locations of grid edges in the OGF since the integer information is incorrectly solved. The examples of the ridge error can be seen in [20] and the Experiments section of this paper [Figs. 7(c) and 8(b)].

In [20], the additional binary fringes with the phase shift of π to the original ones are projected to solve a similar problem, but this doubles the number of fringe images necessary to be captured. Here, we propose a pseudo-phase-shift strategy to solve this problem without any extra image capture requirements.

As shown in Fig. 4(a), it is easy to see the same locations of the ridge errors in the unwrapped phase, the integer phase derived from the OGF, and the phase jump in the wrapped phase. For the integer phase and the wrapped phase, the ridge errors are in the steep area, which makes them difficult to correct by the neighbor points with accurate values. Therefore, they should be “moved” to a smooth area in a reliable reference, which will be calculated from the wrapped phase with a phase shift of π compared with the original one. This shifted phase can be obtained from the phase shift fringes by a modified PSA as

$$\varphi'_W = \tan^{-1} \frac{\sum_{n=1}^N s_n \sin \left(\frac{2\pi n}{N} + \pi\right)}{\sum_{n=1}^N s_n \cos \left(\frac{2\pi n}{N} + \pi\right)}, \quad (16)$$

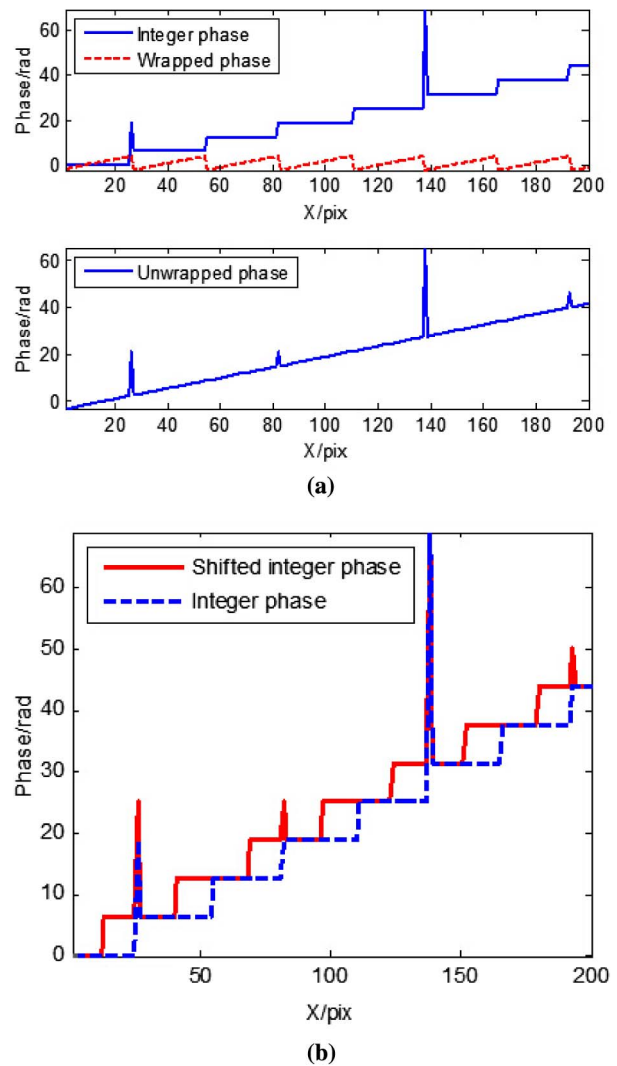


Fig. 4. Pseudo-phase-shift method. (a) Integer phase and unwrapped phase with ridge errors. (b) Ridge errors move to the smooth areas in the shifted integer phase.

where the phase shift values are also assumed uniform in one period as Eq. (12). The deviation between the shifted wrapped phase and the unwrapped phase with error, or the shifted integer phase for short, is shown in Fig. 4(b), which has been added by π to keep the agreement with the original integer phase. It is evident that these two functions are similar but have a spatial displacement of half-fringe period, which means the error is concentrated in the smooth area in the shifted integer phase and absent from the steep area of the nonshifted original one. This property makes the error areas simple to rectify by marking them as invalid. This is achieved by examining the absolute values of wrapped phase and marking those greater than a given threshold. Then, these invalid points can be replaced by the neighborhood of the shifted integer values using the standard image processing methods such as the morphological closing calculation [27]. In practice, the invalid points should be set to zero, and then the gray-scale closing calculation is executed to the shifted integer phase as

$$(\Delta\varphi_w \oplus B) \ominus B \\ = \min\{\max[\Delta\varphi_w(x + x', y + y') | (x', y') \in B]\}, \quad (17)$$

where $\Delta\varphi_w$ is the shifted integer phase, B is the template, and the operators $\min(-)$ and $\max(-)$ represent obtaining the minimum and maximum values. The operators \oplus and \ominus are the gray-scale dilate and erode operators, respectively, which are combined to express the closing calculation. The radius of B should be greater than the maximum half-width of the “gaps” in $\Delta\varphi_w$ caused by the invalid points, so that they can be filled in.

To conclude, the core of this correction method is to generate a reliable reference by a pseudo-shifted wrapped phase while not the real one, so the unwrapped phase can be improved without any increase in the number of fringe images necessary to be captured. The correction effect will be demonstrated in the following section.

D. Measurement Time Comparison

In this subsection, we attempt to give a measurement time comparison between the OGF method and the traditional TPU. It is necessary to emphasize that in this subsection the “capture time” considers the fringes captured for the unwrapping and obtaining the wrapped phases (by phase shift technique) because the whole measurement time is merited here. In addition, we define the parameter M as the category amount of the spatial frequencies for the concision purpose.

To make the comparison more comprehensive, various data-processing modes and hardware conditions are considered. Generally, there are two data-processing modes in the measurement of FRT.

1. Direct processing mode [3]: The fringes in one measurement are projected, captured, and then processed to immediately obtain the phases. In this case, the capture time and calculation time should be focused on, which will be analyzed, respectively, below.

2. Post-processing mode [2,4]: The necessary fringes of many measurements are successively projected, captured, and written to the storage medium (such as the hard disk), which will be processed after the measurements. In this case,

Table 1. Consuming Time of Each Operation in OGF Method and Traditional TPU

Operation Type	Consuming Time (s)	Operation Times in One Measurement	
		OGF Method	Traditional TPU
3-step PSA	0.047 s	2	2M
4-step PSA	0.045 s		
Phase unwrapping based on the gray-level identification [Eq. (9) to Eq. (12)]	0.036 s	2M	—
Closing calculation [Eq. (17)]	0.20 s	2M	—
Summary (s)		0.09 + 0.236M	0.09M

the fringes capture time (including the data recording) is the only important factor to be considered while the relative slow calculation is acceptable.

The capture time of one frame can change dramatically for different hardware conditions, such as the reflective index of the specimen, the data-transmission method, and the sensitivity of the camera. For example, when the reflective index of the specimen and the camera sensitivity are both low, the capture time could be really long. In one of our tests, a glass specimen (without high reflective coating) is measured, and a normal commercial CMOS camera is used to capture the fringes. With these conditions, the capture time of one frame is even greater than 0.5 s. On the other hand, the capture speed can achieve about 10 ms/frame with the special devices prepared for the high-speed measurements [17].

The direct-processing mode will be analyzed at first, where the calculation time of the two methods should be known. The operation to obtain the wrapped phases with different frequencies from phase shift fringes is the major component of the traditional TPU calculation, where the three-step [5] and four-step [4] PSAs are most commonly used. While the OGF

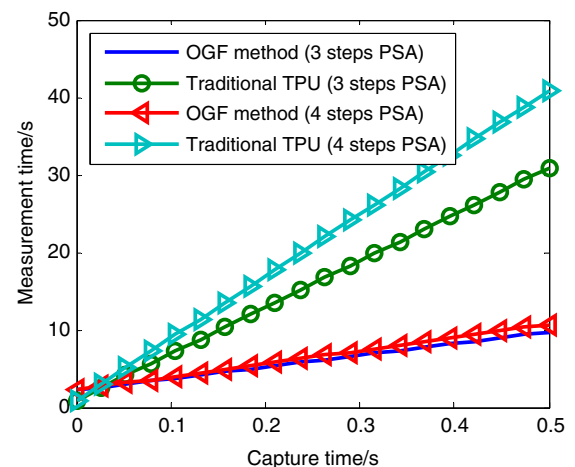


Fig. 5. Consuming time comparison between the OGF method and the traditional TPU (in the case of $M = 6$).

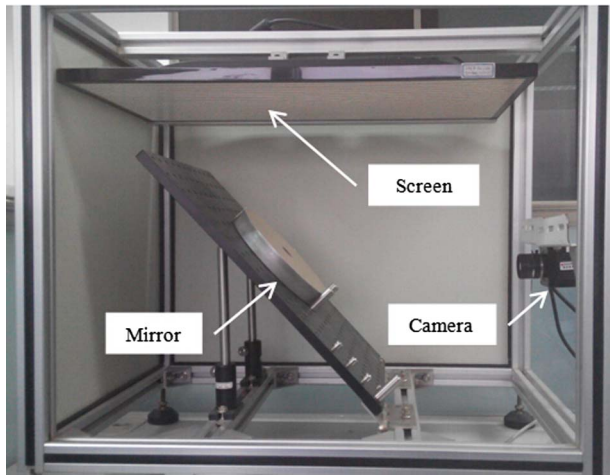


Fig. 6. FRT experiment setup with an annular mirror under test.

method mainly contains the phase unwrapping operation based on the gray-level identification [Eq. (9) to Eq. (12)] and the morphological closing operation [Eq. (17)]. Therefore, we can merit the speed of our method and that of traditional TPU by comparing the time consumption of all three types of operations.

We do the simulations on a laptop computer with the CPU of Intel Core i-7 2640M (2.8 GHz) and 3 GB available RAM. All operations are programmed on the MATLAB R2010a platform, and the tic/toc commands are used to obtain the operation time, where each type of operation is executed 100 times, and the average running time is recorded to make the results more reliable. For simplicity, the fringes' image resolution is set to the fixed value of 1024×768 .

The simulation results are shown in Table 1, where the consuming time of each operation and the summary time of the two methods in one FRT measurement are presented. The two

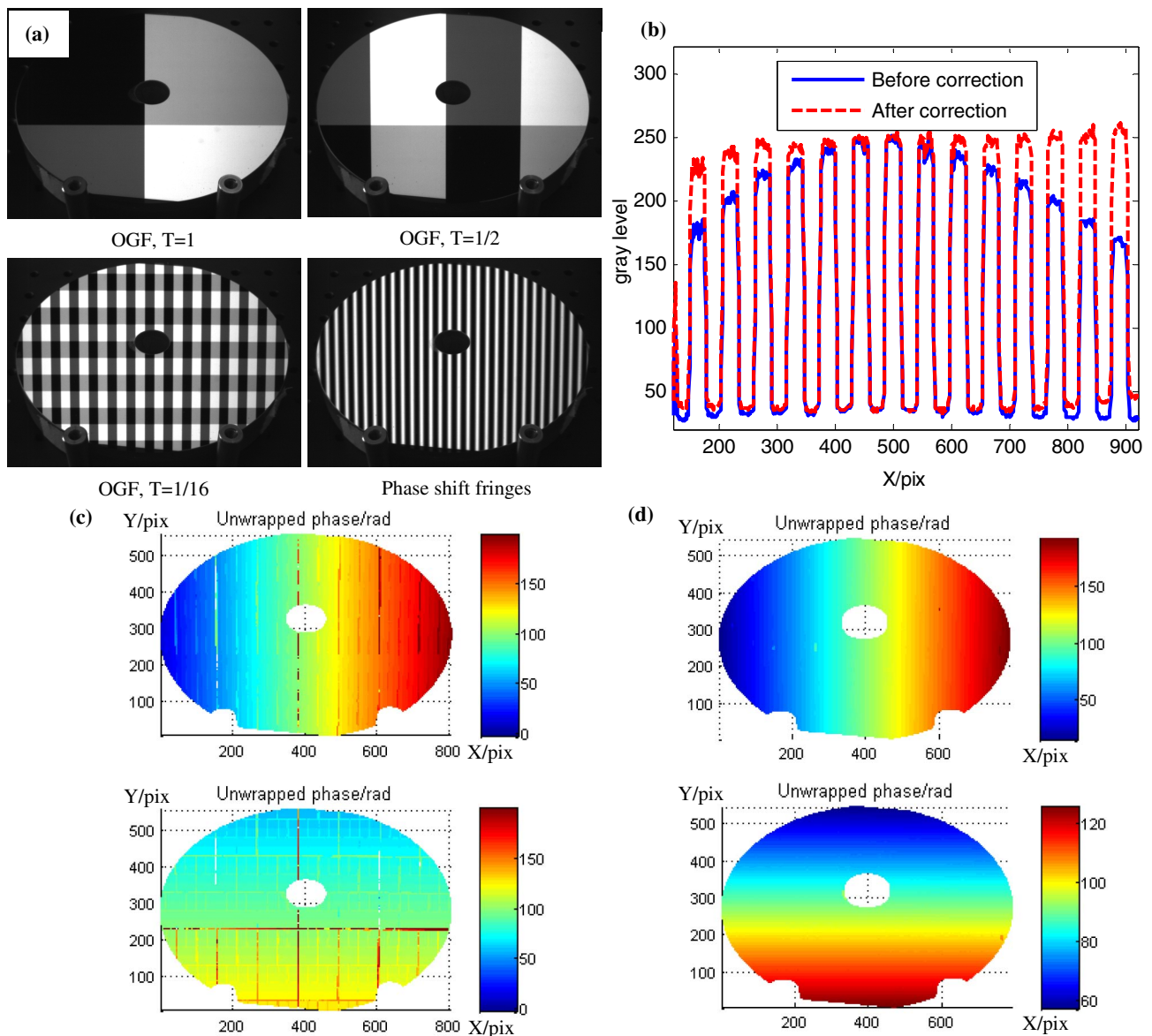


Fig. 7. Experiment to test a plane mirror. (a) Captured OGF and phase shift fringes. (b) Intensity nonuniform correction. (c) Direct unwrapped phases with ridge errors. (d) Phases corrected by the pseudo-phase-shift strategy.

kinds of PSAs have almost the same speed, so their consuming time is not discussed separately. It is notable that the calculation speed of morphological closing is relative to the structuring element (template) size, which is set to 10×10 here, since it is large enough for most cases with fringes image size of 1024×768 .

Now we can provide a time-performance comparison by adding the calculation time to the capture time, which is shown in Fig. 5. Here, M equals to 6, which is the same as in the Experiments section. It is evident that the four measurement time curves are all linear relative with the capture time of one frame. Our OGF method is slower in the case of high-speed capture, but this situation is reversed when the capture time is greater than a threshold (about 0.03 s or 0.02 s using three- or four-step PSA). The speed of OGF method can be approximately 2.5 to 3 times the traditional TPU when the capture time increases to 0.5 s/frame.

On the other hand, in the post-processing mode, the OGF method is always faster than the traditional TPU, since the calculation time is not concerned. For the cases of using three- and four-step PSAs, the measurement time ratio between the OGF and traditional TPU are $(5 + M)/6M$ and $(7 + M)/8M$, which is independent on the capture time. They are 1/3.3 and 1/3.7, respectively, with the substitution $M = 6$. Besides, this acceleration effect also increases with larger M , similarly as the direct-processing mode.

Based on the analysis of this subsection, we can obtain two conclusions:

1. The OGF method is faster than the traditional TPU except for the case of high-speed capture (faster than 0.03 s/frame) in the direct-processing mode of FRT measurement, and it is always faster than the latter in the post-processing measurement mode. Furthermore, the threshold can be reduced by using a more powerful computer to meet the requirement of high-speed measurement.

2. The acceleration ratio of OGF will increase with larger M in both measurement modes, while it is affected by the capture time only in the direct-processing mode.

3. EXPERIMENTS

The experiments are presented in this section to validate our algorithm. To clearly show the effects of the two enhancement strategies, a simple object is tested at first, which is an annular plane mirror with the outside diameter of 160 mm and the inner diameter of 20 mm. The FRT system with the plane mirror is shown in Fig. 6, where the resolution of the camera is 1024×768 and the focal length of the lens is 8 mm. Five OGF fringes with the frequencies of exponential sequence, which means the fringes periods T are from 1 to 1/16 if the screen size is normalized to one, are used to unwrap the phases obtained from the phase shift fringes ($T = 1/32$) [some of these fringes are shown in Fig. 7(a)]. In Fig. 7(b), the curvatures of phase shift fringes before and after nonuniform correction of Section 2.B are both presented for comparison purposes. It can be seen that the spatial uniformity of fringes intensity is significantly improved, so the extraction of integer wrapped phase can be executed using global thresholds, as in Eqs. (9) and (10). The direct unwrapped phases in Eq. (11) are shown in

Fig. 7(c) with many ridge errors, as analyzed in Section 2.C, which are effectively corrected by our pseudo-phase-shift strategy. The refined unwrapped phases are shown in Fig. 7(d).

In the second experiment, the test mirror is unchanged, but the camera lens is defocused largely to obtain the OGF images with severe blur, where the partial image is shown in Fig. 8(a). The intensity curvature of its central row is also illustrated. It can be seen that the grid edges in the captured OGF are blurry and that the curvature shape is even similar as a sinusoid function while not the rectangle one in the ideal case. The outcome of this experiment is to examine the algorithm robustness when the imaging defect of the FRT system is large, since the camera lens is focused on the test mirror rather than the screen. On the top of Fig. 8(b), there are ridge errors in the direct unwrapped phase with significantly larger width compared with Fig. 7(c)

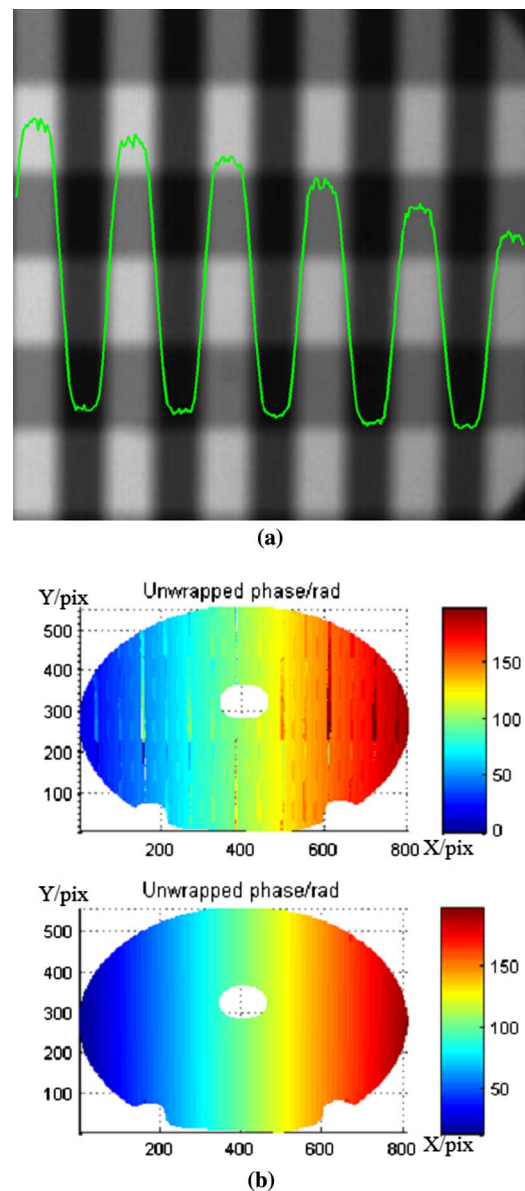


Fig. 8. (a) Captured OGF with large defocusing (partial image). (b) Unwrapped phase before correction (top) and after correction (bottom).

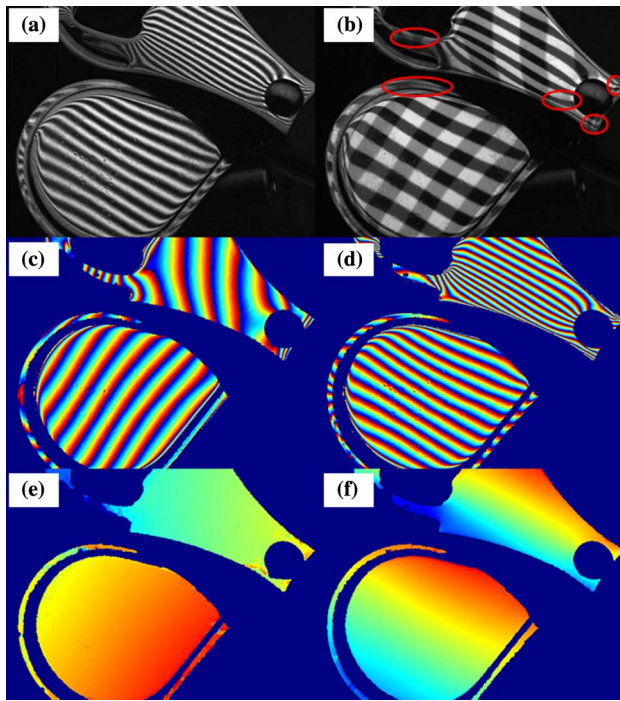


Fig. 9. Algorithm performance for the complex specimen. (a) Captured phase shift fringes. (b) Captured OGF image. (c) and (d) Wrapped phases of the slopes along x and y directions. (e) and (f). Unwrapped phases of (c) and (d).

because of the increase of the points with gray-level ambiguity. However, as shown on the bottom of Fig. 8(b), these errors also can be suppressed well by the pseudo-phase-shift strategy with a larger radius template (about twice as the former experiment) in the morphological closing.

In the last experiment, we choose an unfolded nail clipper as the specimen. As shown in Fig. 9(a), the challenge is much more difficult than the former two experiments due to the high dynamic range of the phase, complex pupil, low contrast area caused by the dirt and scratches on the specimen surface, and the irregular intensity variance. Here, the intensity and contrast distribution are not regular, and the correction method in Section 2.B is unavailable. Three calibration images with uniform gray levels should be projected to overcome this problem, as previously explained, and then the unwrapping algorithm also works well in most areas. The minor phase unwrapping errors occur in the small area with a serious signal-to-noise ratio and very low contrast, as flagged in Fig. 9(b), but it does not spread due to the advantage of TPU. It also can be seen that the unwrapping phase of the y -direction slope in Fig. 9(f) shows the better noise suppression ability than that of the x -direction slope in Fig. 9(e). The reason is that the gray-level identification tolerance of the y direction is looser than that of the x direction in the OGF, deduced by Eq. (9). However, in most cases, the unwrapping robustness of both directions in our algorithm is acceptable, as verified by the experiments.

4. CONCLUSION

In this paper, we introduce the OGF technique into the TPU method to rapidly unwrap a pair of wrapped phases in the

fringe reflection measurements. Based on the combination of two binary fringes into one OGF image, the wrapped phases of one frequency can be obtained using only one captured image. Besides, its robustness is significantly improved by the pseudo-phase-shift strategy without any extra captured fringes. These properties make the necessary amount of captured fringes for TPU operation reduce to 1/4 of the binary fringes method, as well as 1/6–1/8 of the traditional TPU algorithm. The algorithm performance is validated by the experiments, which can work well in the cases of large defocusing. It is also suitable for the complex specimen with a large dynamic range, irregular and discontinuous pupils, and some surface defects. Although three extra calibration images are necessary in this case, the total amount of captured images is still significantly less than in other traditional TPU algorithms.

Funding. National Natural Science Foundation of China (NSFC) (11303068); Natural Science Foundation of Jiangsu Province (Jiangsu Provincial Natural Science Foundation) (BK20131060); Opening Project of Key Laboratory of Advanced Optical Manufacturing Technologies of Jiangsu Province (Soochow University) (KJS1305); the Opening Project of Key Laboratory of Astronomical Optics & Technology (Nanjing Institute of Astronomical Optics & Technology, Chinese Academy of Sciences) (CAS-KLAOT-KF201303).

REFERENCES

1. Y. Y. Hung, L. Lin, H. M. Shang, and B. G. Park, "Practical three-dimensional computer vision techniques for full-field surface measurement," *Opt. Eng.* **39**, 143–149 (2000).
2. T. Bothe, W. S. Li, C. von Kopylow, and W. Juptner, "High-resolution 3D shape measurement on specular surfaces by fringe reflection," *Proc. SPIE* **5457**, 411–422 (2004).
3. M. C. Knauer, J. Kaminski, and G. Hausler, "Phase measuring deflectometry: a new approach to measure specular free-form surfaces," *Proc. SPIE* **5457**, 366–376 (2004).
4. P. Su, R. E. Parks, L. R. Wang, R. P. Angel, and J. H. Burge, "Software configurable optical test system: a computerized reverse Hartmann test," *Appl. Opt.* **49**, 4404–4412 (2010).
5. Y. L. Xiao, X. Y. Su, W. J. Chen, and Y. K. Liu, "Three-dimensional shape measurement of aspheric mirrors with fringe reflection photogrammetry," *Appl. Opt.* **51**, 457–464 (2012).
6. J. Burke, W. Li, A. Heimsath, C. von Kopylow, and R. B. Bergmann, "Qualifying parabolic mirrors with deflectometry," *J. Eur. Opt. Soc.* **8**, 13014 (2013).
7. J. M. Huntley and H. Saldner, "Temporal phase-unwrapping algorithm for automated interferogram analysis," *Appl. Opt.* **32**, 3047–3052 (1993).
8. J. M. Huntley and H. O. Saldner, "Error-reduction methods for shape measurement by temporal phase unwrapping," *J. Opt. Soc. Am. A* **14**, 3188–3196 (1997).
9. H. O. Saldner and J. M. Huntley, "Temporal phase unwrapping: application to surface profiling of discontinuous objects," *Appl. Opt.* **36**, 2770–2775 (1997).
10. J. Tian, X. Peng, and X. Zhao, "A generalized temporal phase unwrapping algorithm for three-dimensional profilometry," *Opt. Laser Eng.* **46**, 336–342 (2008).
11. D. C. Ghiglia and M. D. Pritt, *Two-Dimension Phase Unwrapping: Theory, Algorithms and Software* (Wiley, 1998).
12. R. M. Goldstein, H. A. Zebker, and C. L. Werner, "Satellite radar interferometry—two-dimensional phase unwrapping," *Radio Sci.* **23**, 713–720 (1988).
13. X. Su and W. Chen, "Reliability-guided phase unwrapping algorithm: a review," *Opt. Lasers Eng.* **42**, 245–261 (2004).

14. D. C. Ghiglia and L. A. Romero, "Robust two-dimensional weighted and unweighted phase unwrapping that uses fast transforms and iterative methods," *J. Opt. Soc. Am. A* **11**, 107–117 (1994).
15. M. D. Pritt and J. S. Shipman, "Least-squares 2-dimensional phase unwrapping using FFTs," *IEEE Trans. Geosci. Remote Sens.* **32**, 706–708 (1994).
16. H. Zhang, L. Ji, S. Liu, S. Li, S. Han, and X. Zhang, "Three-dimensional shape measurement of a highly reflected, specular surface with structured light method," *Appl. Opt.* **51**, 7724–7732 (2012).
17. H. Nguyen, D. Nguyen, Z. Wang, H. Kieu, and M. Le, "Real-time, high-accuracy 3D imaging and shape measurement," *Appl. Opt.* **54**, A9–A17 (2015).
18. J. M. Huntley and H. O. Saldner, "Shape measurement by temporal phase unwrapping: comparison of unwrapping algorithms," *Meas. Sci. Technol.* **8**, 986–992 (1997).
19. G. Sansoni, M. Carocci, and R. Rodella, "Three-dimensional vision based on a combination of gray-code and phase-shift light projection: analysis and compensation of the systematic errors," *Appl. Opt.* **38**, 6565–6573 (1999).
20. G. P. Butel, G. A. Smith, and J. H. Burge, "Binary pattern deflectometry," *Appl. Opt.* **53**, 923–930 (2014).
21. P. Xie, M. Tang, and X. Wei, "Three-dimensional shape measurement of specular surfaces by orthogonal composite fringe reflection," *Proc. SPIE* **8200**, 820014 (2011).
22. L. Huang, C. S. Ng, and A. K. Asundi, "Dynamic three-dimensional sensing for specular surface with monoscopic fringe reflectometry," *Opt. Express* **19**, 12809–12814 (2011).
23. D. Malacara, M. Servin, and Z. Malacara, *Interferogram Analysis for Optical Testing* (Taylor & Francis, 2005).
24. H. W. Guo, H. T. He, and M. Chen, "Gamma correction for digital fringe projection profilometry," *Appl. Opt.* **43**, 2906–2914 (2004).
25. J. A. Quiroga and M. Servin, "Isotropic n -dimensional fringe pattern normalization," *Opt. Commun.* **224**, 221–227 (2003).
26. T. Kreis, "Digital holographic interference-phase measurement using the fourier-transform method," *J. Opt. Soc. Am. A* **3**, 847–855 (1986).
27. R. C. Gonzalez, R. E. Woods, and S. L. Eddins, *Digital Image Processing Using MATLAB* (Gatesmark, 2009).